Chapter 8

Mechanical and Tribological Properties of Plasma Deposited a-C:H:Si:O Films

Bruno B. Lopes, Rita C.C. Rangel, César A. Antonio,
Steven F. Durrant, Nilson C. Cruz, Elidiane C. Rangel

Additional information is available at the end of the chapter

http://dx.doi.org/10.5772/50278

1. Introduction

Plasma deposited organosilicon films (a-C:H:Si:O) have attracted increasingly attention due to superior properties such as good adhesion (Morent *et al.*, 2009), optical transparency (Zajíčková et al., 2001), corrosion resistance (Rangel et al., 2012) and selective permeability (Czeremuszkin et al., 2001). Moreover, highly hydrophilic to extremely hydrophobic films can be prepared by properly adjusting the plasma excitation conditions (Schwarz et al., 1998). Such selectable wettability combined with the optical transparency and chemical inertness make these films potential candidates for a series of applications including haemocompatible (Ong et al., 2007), biocompatible (Ong et al., 2008), and corrosion protective (Fracassi et al., 2003) coatings, fire retardants (Quédé et al., 2002), diffusion barriers (Görbig et al., 1998), adherent (Pihan et al., 2009) and non-adherent surfaces (Navabpour et al., 2010), and dielectric layers (Borvon *et al.*, 2002). Although the literature is abundant in reports of improvements upon the application of a-C:H:Si:O films, only a few studies dealt with the mechanical and tribological properties of such coatings, characteristics of fundamental relevance to the durability of the coating. In this context, this article describes an investigation of the mechanical and tribological properties of silicon containing organic coatings deposited by Plasma Enhanced Chemical Vapor Deposition from hexamethyldisiloxane, HMDSO, and oxygen mixtures. The effect of the dilution of HMDSO in oxygen on the hardness and elastic modulus was accessed by nanoindentation. Friction coefficient, scratching and wear resistances of the films were also evaluated via scratching tests performed with the same instrument used for nanoindentation. Topography and morphology of the films as well as their average roughnesses were determined from scanning probe microscopy images.

2. Experimental details

Figure 1 illustrates the experimental setup employed in the treatments. It consists of a cylindrical glass chamber, of 190 mm internal diameter and 250 mm high, sealed by aluminum plates and fitted with two parallel electrodes. Prior to the depositions glass substrates were sonicated in detergent solution and acetone baths and then dried using a hot air gun. Subsequently, they were sputter-cleaned for 600 s in plasmas established in atmospheres of 50% Ar /50% H_2 at a total pressure of 1.33 Pa. The sputtering plasmas were produced by the application of radiofrequency power, RF, (13.56 MHz, 150 W) to the lower electrode which also serves as substrate holder while the steel mesh used as the upper electrode was grounded. The depositions were performed for 3.600 s in atmospheres of pure HMDSO or 30% of HMDSO and 70% of O_2 by applying RF (13.56 MHz, 200 W) to the substrate holder. In all the experiments, the total gas pressure was kept at 20 Pa.

Film thickness was determined from film step heights, which were delineated on glass surfaces using a mask of Kapton tape during the depositions. The height of the steps was measured in three different regions using a Veeco Dektak 150 profilometer. Chemical composition and structure of films deposited onto aluminum-coated glass slides were investigated by infrared reflectance-absorbance spectroscopy using a Jasco FTIR-410 spectrometer. Each spectrum is the result of the addition of 124 spectra acquired with a resolution of 4 cm^{-1}. The coating mass was measured by weighing the substrates before and after the deposition, while the coating volume was evaluated from the substrate area and film thickness, thus allowing the determination of its density. The effect of the percentage of O_2 on the hardness and the elastic modulus of the coatings was assessed by the Oliver and Pharr method (Oliver et al., 1992) using load displacement curves obtained from nanoindentation experiments undertaken using a Hysitron TriboIndenter. At least 9 measurements were conducted on each sample using a multiple load function applied to a diamond Berkovich tip with maximum loads from 1000 to 10000 μN. The application rate at the maximum load varied from 36 (1000 μN) to 360 μN/s (10000 μN). A dwell time of 1 s was used throughout. Scratch experiments were conducted by associating the normal and lateral force capabilities of the nanoindenter. The friction coefficient was determined from 10 μm-long scratches produced by the application of a normal load of 300 μN on the indenter tip. The tip speed and the load application rate were 1 μm/s and 150 μN/s, respectively. A second batch of 10 μm-long scratches was obtained to investigate the scratching resistance of the films. Prior to the test, to evaluate the initial surface condition, the 10 μm region was scanned at a normal load of 200 μN applied at 100 μN/s. Subsequently, 5.000 μN was applied to the stationary nanoindenter tip and, as the maximum load was reached, scratching was produced over the 10 μm region for 10 s. The normal load was then reduced to 200 μN and a new scan was performed to probe the tested surface. The wear experiments were conducted using a 19-cycle tooth saw-like function with maximum loads of 1000, 2000, 3000 and 4000 μN. For all the scratching tests mentioned here, at least three experiments were conducted at different positions of each sample. Scanning probe microscopy (SPM) images were acquired in the Hysitron Triboindenter system before and after the nanoindentation, scratching and wear experiments, undertaken by applying 4.0 μN of normal load to the Berkovich tip. The topography and morphology of the films as well

as their average roughnesses were also determined from SPM images of the non-scratched/non-indented areas. Mechanical, tribological and topographical characterizations were all performed in samples prepared on glass plates.

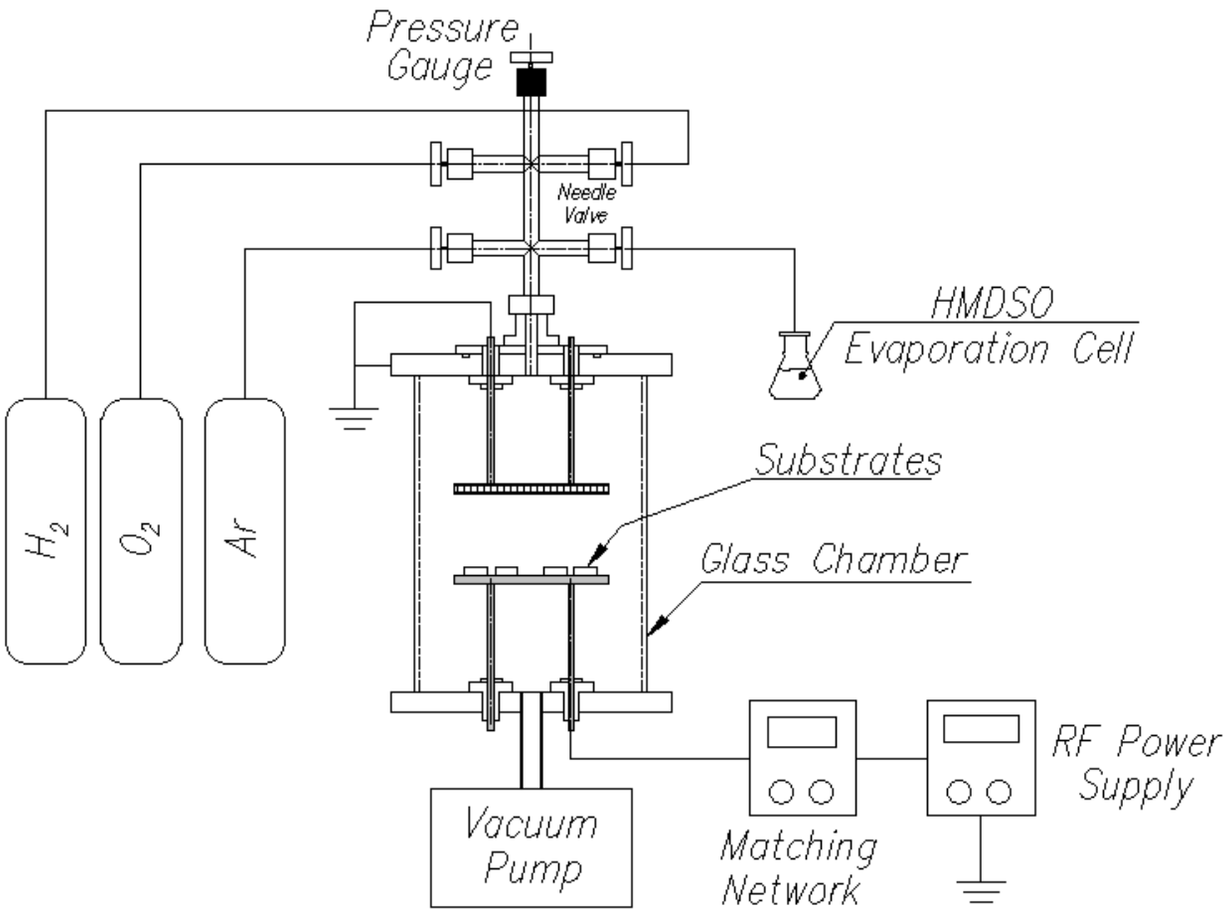

Figure 1. Experimental setup used for substrate cleaning and film deposition.

3. Results and discussions

Figure 2 shows the infrared spectra of films deposited with 0 and 70% of oxygen in the gas feed. Considering the spectrum of the film prepared from a pure HMDSO (0% O_2) plasma, the most prominent absorptions are related to symmetrical C-H stretching vibrations in CH_3 (2959 and 2899 cm^{-1}), to rocking of $(CH)_x$ in $Si(CH_3)_x$ (1262 cm^{-1}), to symmetrical and asymmetrical stretching of Si-O in Si-O-Si (1100 and 1020 cm^{-1}, respectively) and to rocking of CH_3 in $Si(CH_3)_3$ (845 and 750 cm^{-1}) and $Si(CH_3)_2$ (808 cm^{-1}) groups. Lower intensity bands are detected in 2100-2250 (ν Si-H), 1408 (δ C-H in $Si(CH_3)_x$) and 687 (ν $Si-H_n$) cm^{-1}. All the above mentioned absorptions were also observed in similar films studied in previous works (Gengenbach & Griesser, 1999, Rangel et al., 2012, Ul et al., 2002).

A general widening of the bands (3000, 1408, 1262 and 800 cm^{-1}) is observed as oxygen is introduced to the plasma, indicating a higher degree of fragmentation of the organic compound in the presence of higher proportions of active oxygen. Furthermore, the

detection of the stretching mode of the silanol group (3644 cm^{-1}), which is not an original bond of the organometallic molecule, indicates multiple step reactions in the plasma phase. In addition, oxygen incorporation by trapped free-radical grows, as suggested by the emergence of the contributions lying at 3281 (hydrogen bonded O-H) (Ricci et. al., 2011) and 1725 (ν C=O) cm^{-1}. All these changes indicate that oxygen catalyses film deposition, which is readily confirmed by considering the results presented in Fig. 3, that shows an increase in thickness (from 2.2 to 8.3 µm) upon oxygen incorporation. Despite the enlargement of the layer, the intensity of the band related to methylsilyl groups (1262 cm^{-1}) decreases for the film deposited with 70% of oxygen. The loss of Si-connected CH_3 groups enables new points of crosslinking to be established between the Si backbones, increasing the structure density (Pfuch et. al., 2006, Ul et al., 2000). The downshift of the Si-O asymmetric component from 1020 to 993 cm^{-1} is further evidence of film densification (Choudhury et.al., 2010) upon oxygen incorporation. Therefore, all the above discussion suggests that films prepared from pure HMDSO possess a silicone-like structure with Si-H terminations while that deposited from the HMDSO/O_2 mixture is more inorganic, denser and therefore more susceptible to atmospheric oxygen uptake than the former.

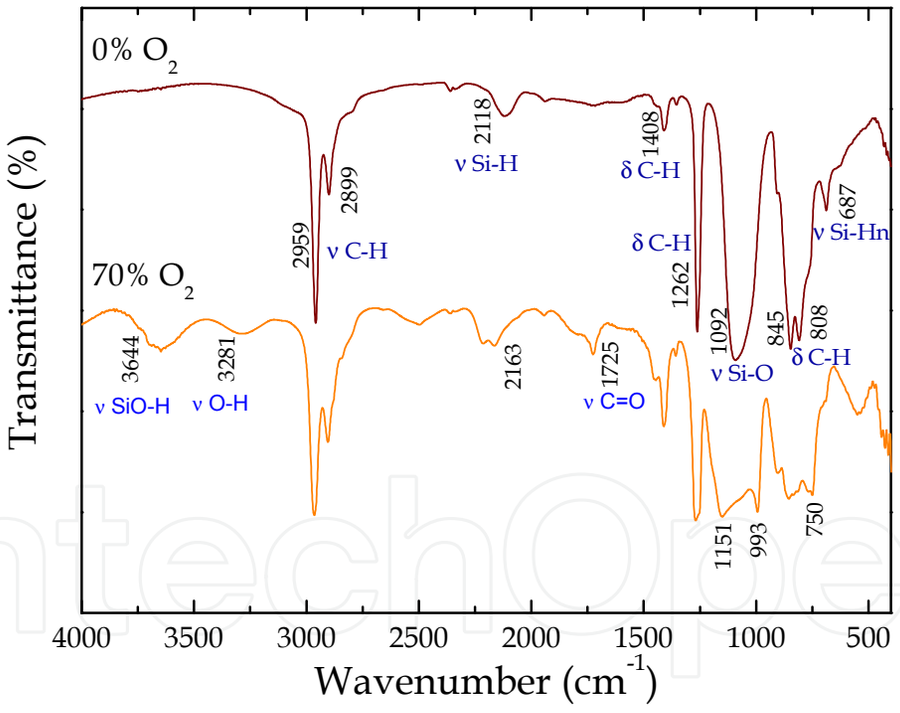

Figure 2. Infrared spectra of films deposited in plasmas with 0 and 70% oxygen.

Besides thickness, Fig. 3 also shows the density of the films. The simultaneous rise in thickness and density suggests that oxygen has a strong influence on the plasma kinetics. Density increases by around 7% (1.83 - 1.96 g/cm^3) as the proportion of O_2 enhances from 0 to 70%. This result is consistent with the loss of the light methyl groups, inducing both crosslinking and enrichment with the inorganic Si-O group. Films derived from HMDSO/O_2 plasma mixtures with densities ranging from 1.4 (polymer-like) to 2.2 g/cm^3 (oxide-like)

have already been obtained in a previous study (Ul et al., 2000) by varying the proportion of oxygen from 0 to 80%. The lower density of the film prepared with the highest oxygen proportion in the present work is attributed to the acceleration in the deposition rate as oxygen is incorporated in the process.

Figure 4 shows 2D topographic images of the samples prepared in this work. Below each image there is a cross-section profile representing the line in the correspondent image. The left-hand images were taken from the sample prepared in pure HMDSO plasmas while those on the right, are from films obtained from HMDSO-O_2 plasmas. Comparing the topmost images (50 X 50 μm^2), the presence of particulates with different diameters spread over a more uniform region is readily observed. The proportion and diameter of the particles substantially rise upon oxygen incorporation, which is reinforced by the 20 X 20 μm^2 profiles (middle position images). As magnification is further increased (lowermost 10 X 10 μm^2 images) it is possible to verify the non-existence of the uniform matrix connecting the particles. In both samples, the structure is granular and the dimension of the particulates increases with increasing oxygen incorporation (line profiles).

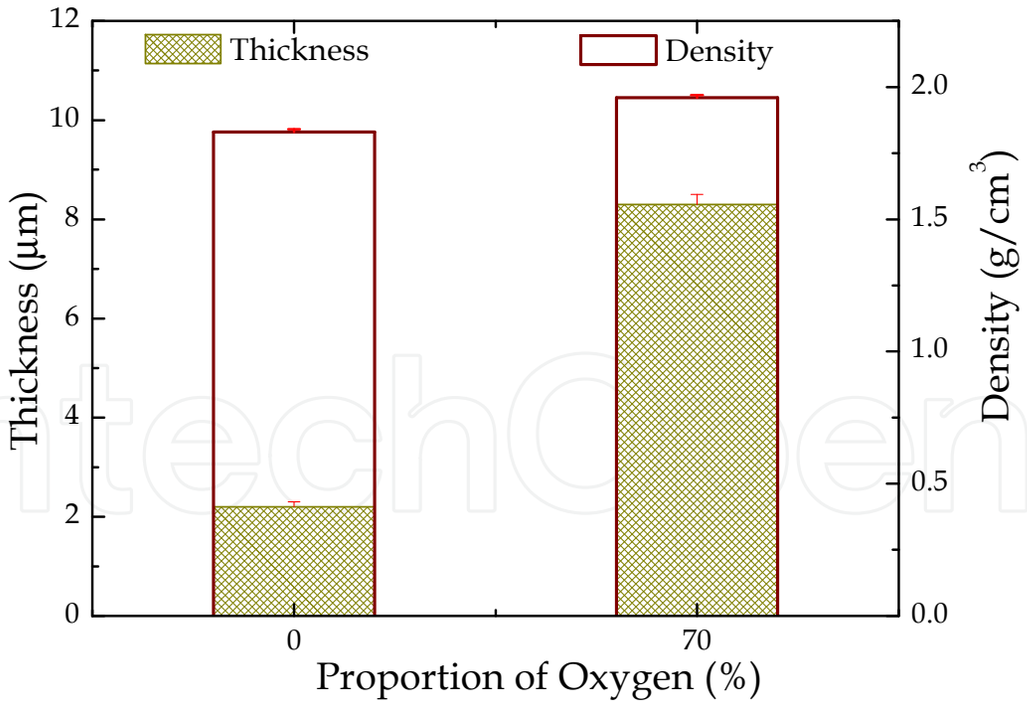

Figure 3. Thickness and density of the films as a function of the proportion of oxygen in the plasma feed.

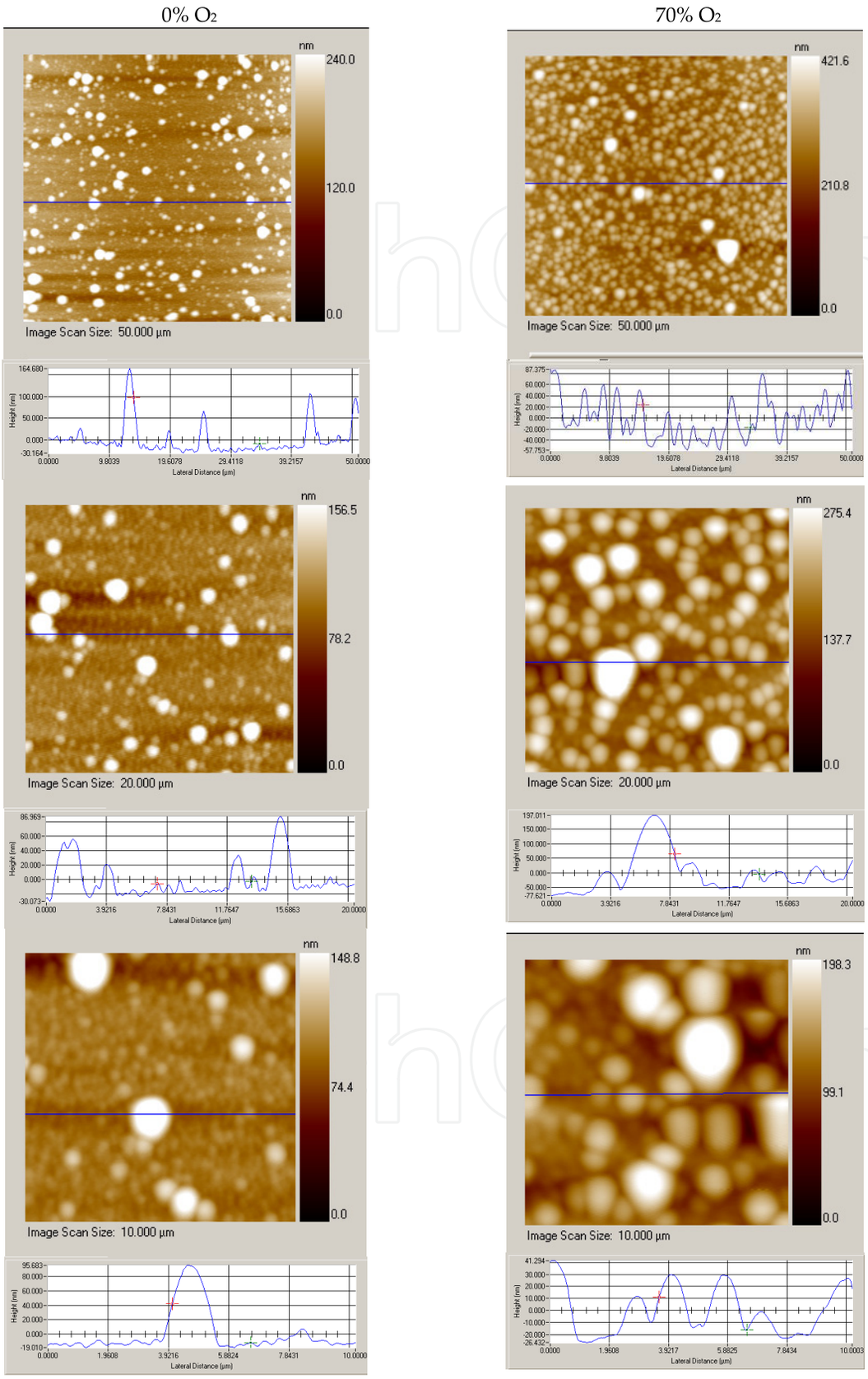

Figure 4. Surface topographical images of the sample deposited in pure HMDSO (left) and in HMDSO/O_2 (right) plasmas acquired at different magnifications.

The analysis of the images suggests that particulates are formed in the highly reactive plasma atmosphere by recombination of the HMDSO fragments. It has already been demonstrated that, under the same plasma condition, the size of the particles evolves with increasing deposition time (Ricci et al., 2011), giving rise to a structure composed of small diameter particles underneath the large diameter ones (lowermost image of Fig.4). The deposition of the macromolecules originates the film in which connections are established by radicals trapped in neighboring structures. As the reactivity of the plasma increases upon oxygen incorporation, the coalescence process accelerates, explaining the deposition of still higher dimensional structures, in equivalent time intervals. Ricci has also demonstrated that oxygen stimulates powder formation in HMDSO/O_2 plasmas (Ricci et al., 2011).

Figure 5 depicts the 3D topographical images of the surfaces derived from the images presented in Fig.4. Even though the height scales are not the same in the graphs, the differences on the surface topography caused by oxygen incorporation are clearly detected as one compares the left-hand to the right-hand images in this picture.

The root mean square roughness of the films, RMS, was evaluated from the 50 X 50 μm^2 total image areas. Figure 6 shows the results as a function of the proportion of oxygen in the plasma feed. The elevation of RMS from 25 to 35 nm is consistent with the growth in the particulate diameters induced by the increase in the deposition rate.

Several works in the literature (Boscher et. al., 2010, Rangel et al., 2012, Rouessac et al., 2011, Ul et al., 2002) report the production of a ball-like structure in films deposited from HMDSO under specific conditions. In none of those works, however, is a detailed characterization of the mechanical properties of this kind of structure provided. Thus, associating the scanning probe microscopy and nanoindentation capabilities of the equipment employed here, the mechanical properties of the films were derived using the Oliver and Pharr method (Oliver et al., 1991).

The images showing the indentation positions before and after the tests and the corresponding multiple load functions generated are depicted in Fig. 7 (0% O_2) and 8 (70% O_2). Although a high load was applied to the indenter (5000 μN), there is no sign of plastic deformation remaining in the images of the surfaces after the tests. The low scattering of the curves in Fig. 7 is surprising as one considers the non uniform nature of the structures studied here. From such curves it is observed that material deforms upon the application of the force but it recovers rapidly as the indenter is withdrawn from the film. From the unloading portion of the curves it can be seen that the material stops pushing the indenter tip, that is, the tip senses a null force, at around 350 nm (Fig.7), which then represents the permanent deformation caused by the indentation. It is also interesting to observe that the residual strain shown in the curves of Fig. 8 is around half (< 150 nm) of that produced in coatings prepared in pure HMDSO plasmas.

Despite its higher roughness, the film deposited in oxygen containing plasmas presented, in general, lower dispersion of the curves (Fig. 8) even if all the 14 load-displacement curves generated for this sample are placed together (Fig. 9a). The good repeatability of the curves then justifies the number of indentation experiments (at least 9) employed. In addition, comparing the areas inside the indentation curves presented in Fig. 9b, reveals a higher recovery rate for the film deposited using 70% of O_2, suggesting a more elastic structure.

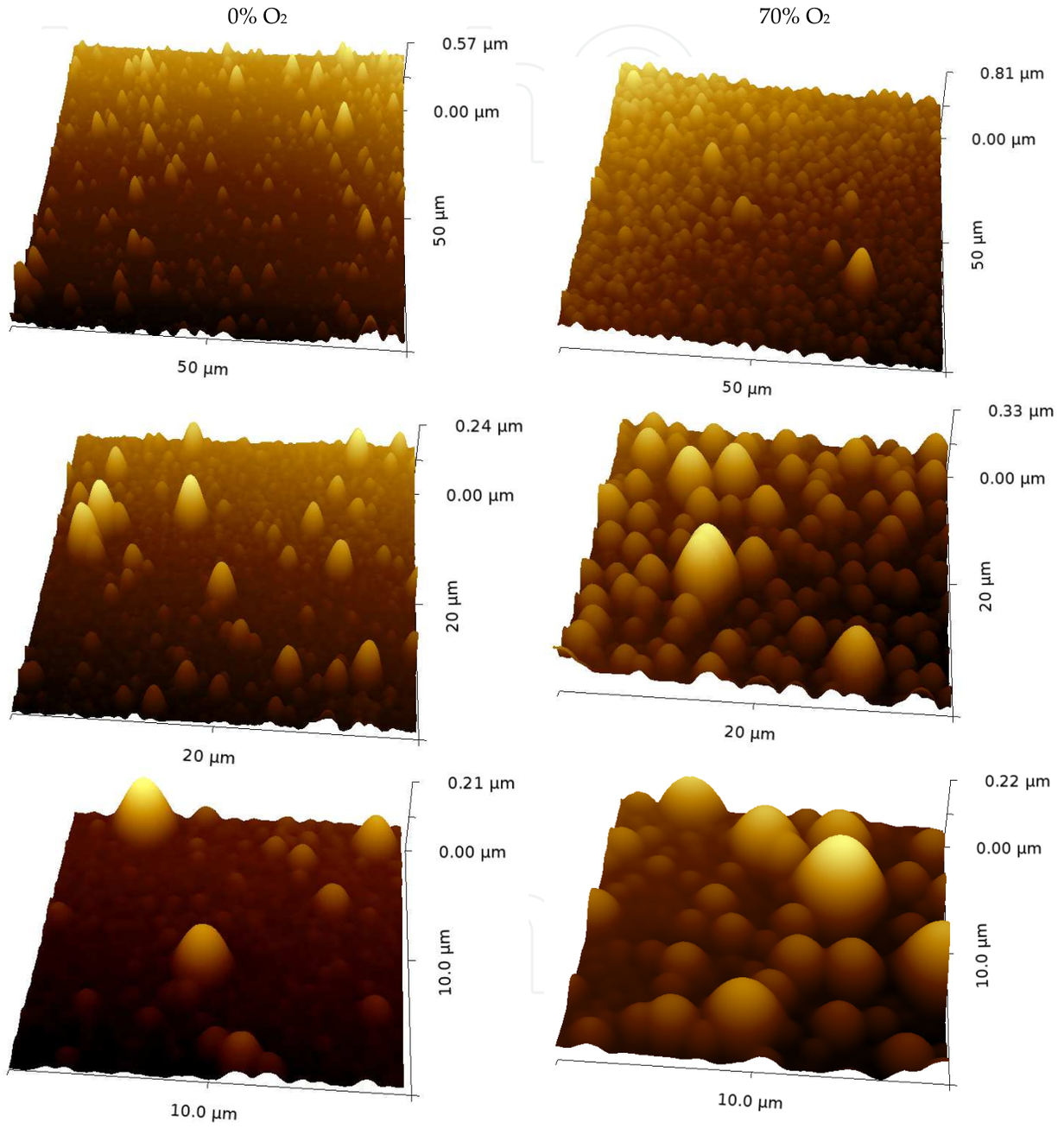

Figure 5. 3D topographical images of the sample deposited in pure HMDSO (left) and in HMDSO/O_2 plasmas (right) taken with different magnifications.

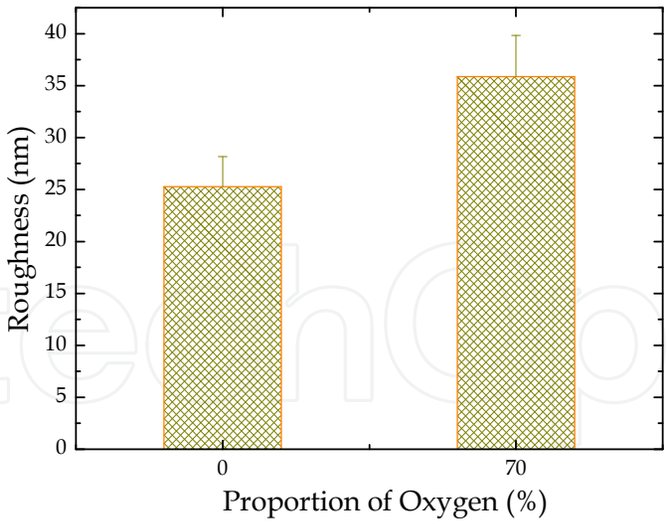

Figure 6. Root mean square roughness the films as a function of the oxygen proportion in the plasma phase.

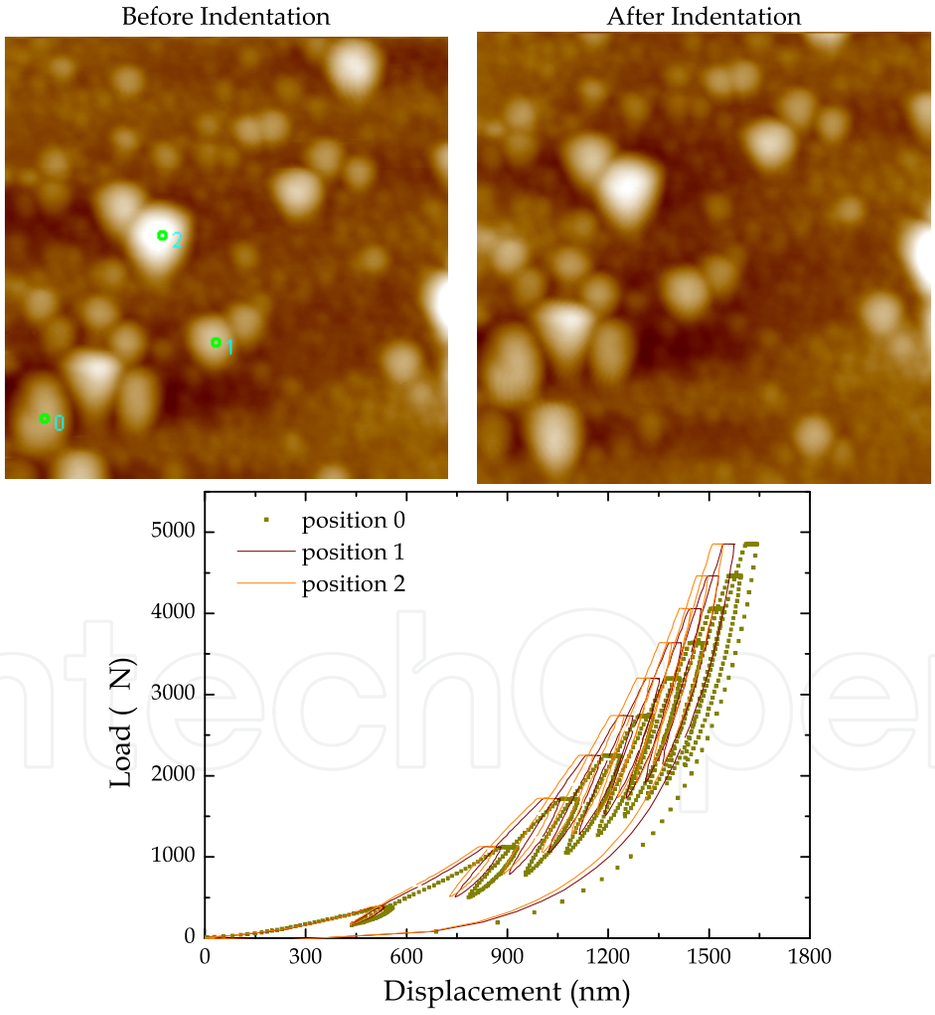

Figure 7. 10 X 10 μm² atomic force microscopy images of the film deposited in plasmas of pure HMDSO: (left) before and (right) after indentation. The points in the left image correspond to the location where the indentations were conducted using 5000 μN maximum load in a multiple load function. The graph at the bottom presents the loading-displacement functions generated at each corresponding point.

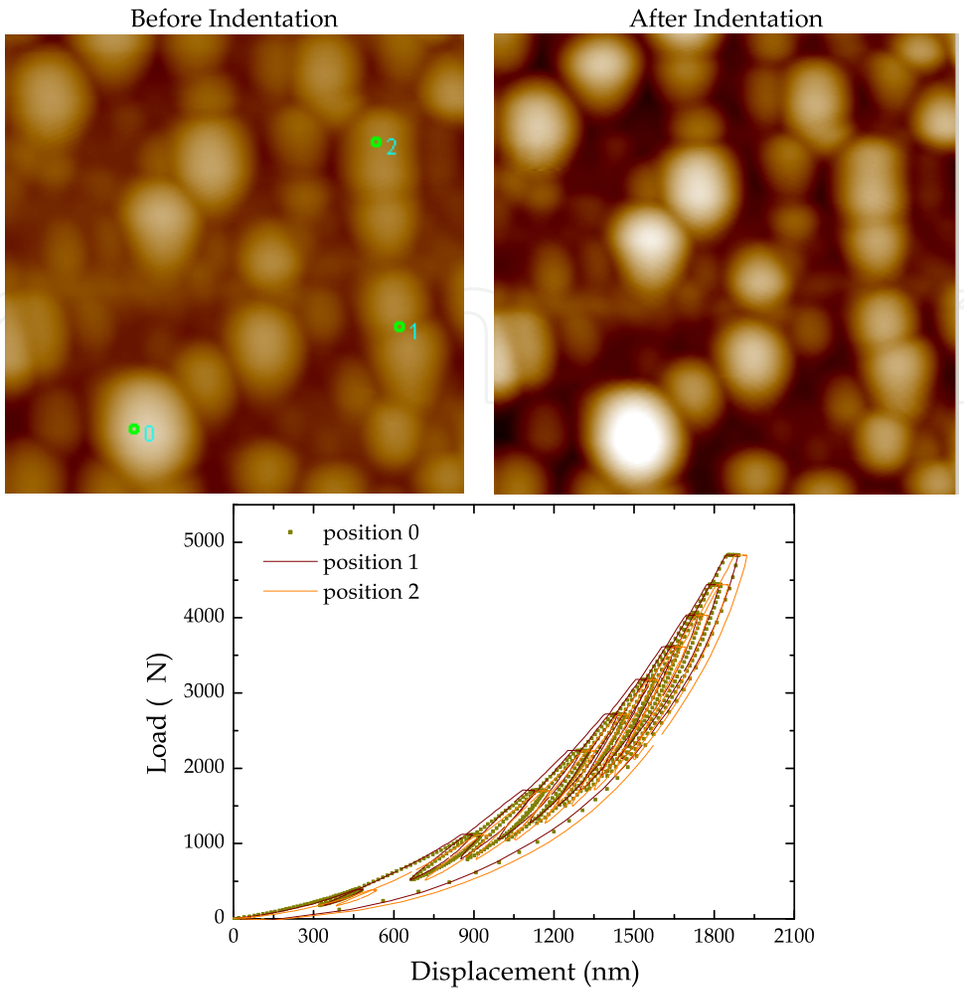

Figure 8. 10 X 10 μm² atomic force microscopy images of the film deposited in plasmas of HMDSO/O_2 mixtures: (left) prior and (right) after indentation. The points in the left image correspond to the location where the indentations were conducted using 5000 μN of maximum load in a multiple load function. The lower graph presents the loading-displacement functions generated in each corresponding point.

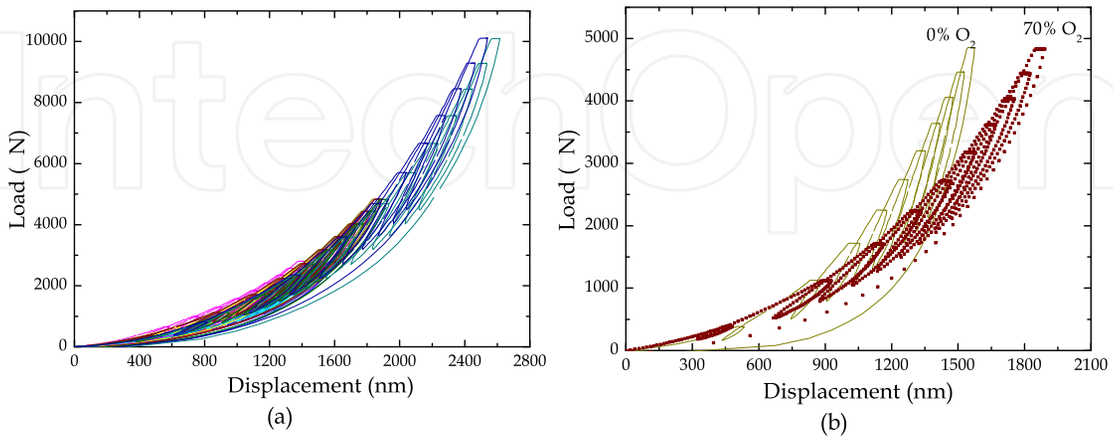

Figure 9. (a) Multiple load functions obtained from the indentations of the sample prepared in oxygen containing plasmas. The maximum loads employed in the experiments were 1000, 3000, 5000 and 10000 μN. (b) Load displacement curves of the samples prepared with 0 and 70% of oxygen in the plasma acquired with 5000 μN of maximum load.

The hardness of the structures was evaluated and is depicted in Fig. 10 as a function of depth for films prepared with 0 and 70% of oxygen in the plasma. Each curve represents data acquired using different loads. For the sample prepared in pure HMDSO plasma, the hardness tends to increase with increasing penetration depth, except for the curve taken using the lowest load (2000 μN). This behavior is ascribed to the growing interference of the mechanical properties of the glass substrate with the results, since the film thickness was 2.2 μm in this case. As the sample deposited with 70% of oxygen is thicker (8.3 μm), no substrate interference is evident but the hardness tends to a fixed value (~ 0.10 GPa) for penetration depths greater than 600 nm. In both graphs, the error bars are observed to decrease with increasing depth due to the greater uncertainties in depth determination as shallower penetrations are employed. Comparing the results obtained at the lowest depth in each sample, presented in the lowermost graph of Fig. 10, one finds that hardness is, on average, greater for the films deposited with oxygen in the plasma phase, which is consistent with the increase in the proportion of oxide groups in the structure.

The hardness values encountered here are around one order of magnitude smaller than those reported for silica-like films (Bewilogua et al., 2011, Choudhury et al., 2011, Jin et al., 2011), but are very similar to those reported for HMDSO plasma deposited films with silicone-like structures (Choudhurya, et al., 2011). Considering such findings, it is possible to infer that the ball-structures are essentially polymeric. This interpretation is corroborated by the results obtained on the glass substrate, presented in Fig.11, which is essentially composed of silica and presents hardness values at least 40 times greater than those encountered for the materials studied here.

Figure 12 shows the reduced elastic modulus as a function of depth for both samples investigated here. Data acquired using different maximum loads are represented by the distinct curves in the graphs. Since the Young's modulus of the film is very low compared to that of the indenter tip, the effect of the tip material on the results will be neglected (Schilde et al., 2012). Therefore, from now on, the reduced elastic modulus will be used as the elastic modulus of the structure. For the thinnest film (0% O_2), the elastic modulus tends to increase with increasing depth in all the curves while the same behavior is detected in the curves of the thicker layer (70% O_2) only at the highest indentation load (10000 μN). Considering the smallest penetration depth in each sample, it is observed that elastic modulus decreases upon oxygen incorporation (lowermost graph); that is, the film gains elasticity as the proportion of oxide groups in the structure increases. The elastic modulus measured for the glass plate, depicted in Fig. 13, presents values more than 40 times greater than those obtained for the films, confirming the polymeric nature of the Si-O containing particles.

Considering that the particulates are finite structures with diameters of some micrometers and that the penetration depth reaches this order of magnitude in some cases, the values found in this work for the mechanical properties do not correspond to those of the particulates but, instead, to the overall film structure. This means that the mechanical properties of the neighboring particulates affect the indentation results obtained in a particular structure and no attempt was made to correct this interference. For depths greater than 15% of the total film thickness, there is also interference owing to the mechanical properties of the glass substrate.

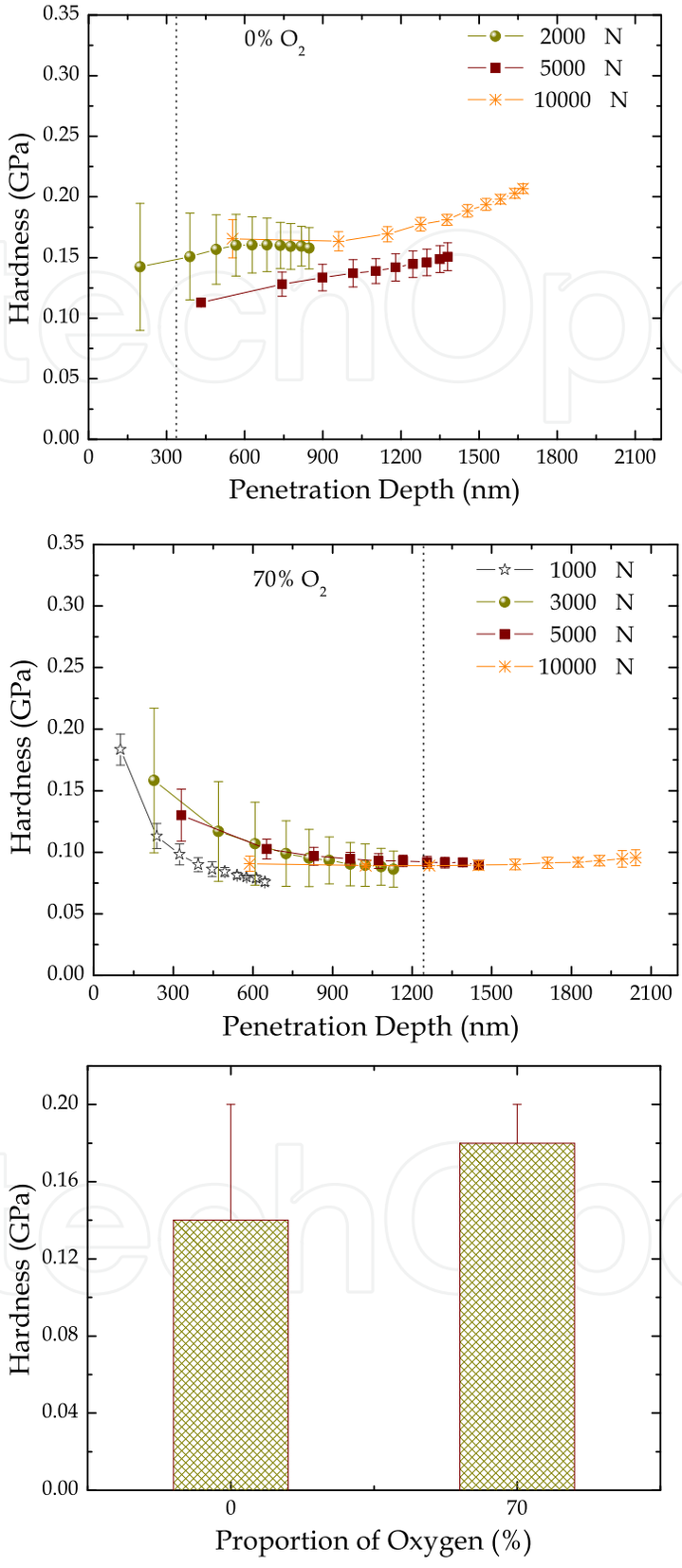

Figure 10. Hardness as a function of depth for films deposited using 0 and 70% of oxygen in the plasma. The vertical dotted lines in the graphs represent 15% of the total film thickness. The lowermost graph presents the hardness of the shallowest region probed in the different samples.

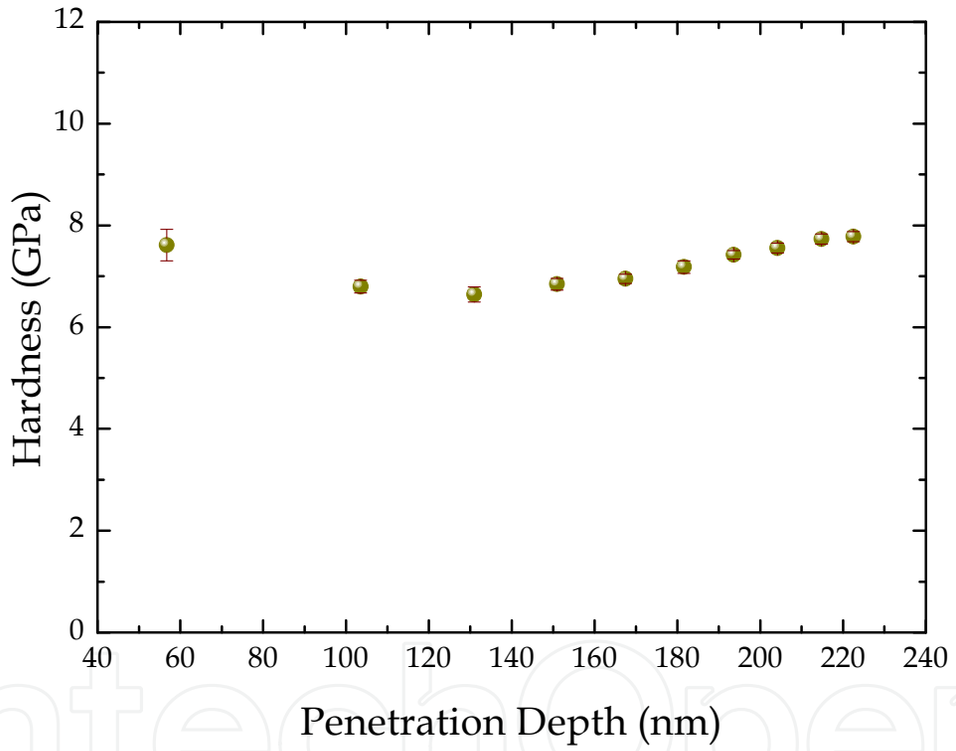

Figure 11. Hardness as a function of the penetration depth for the glass substrate.

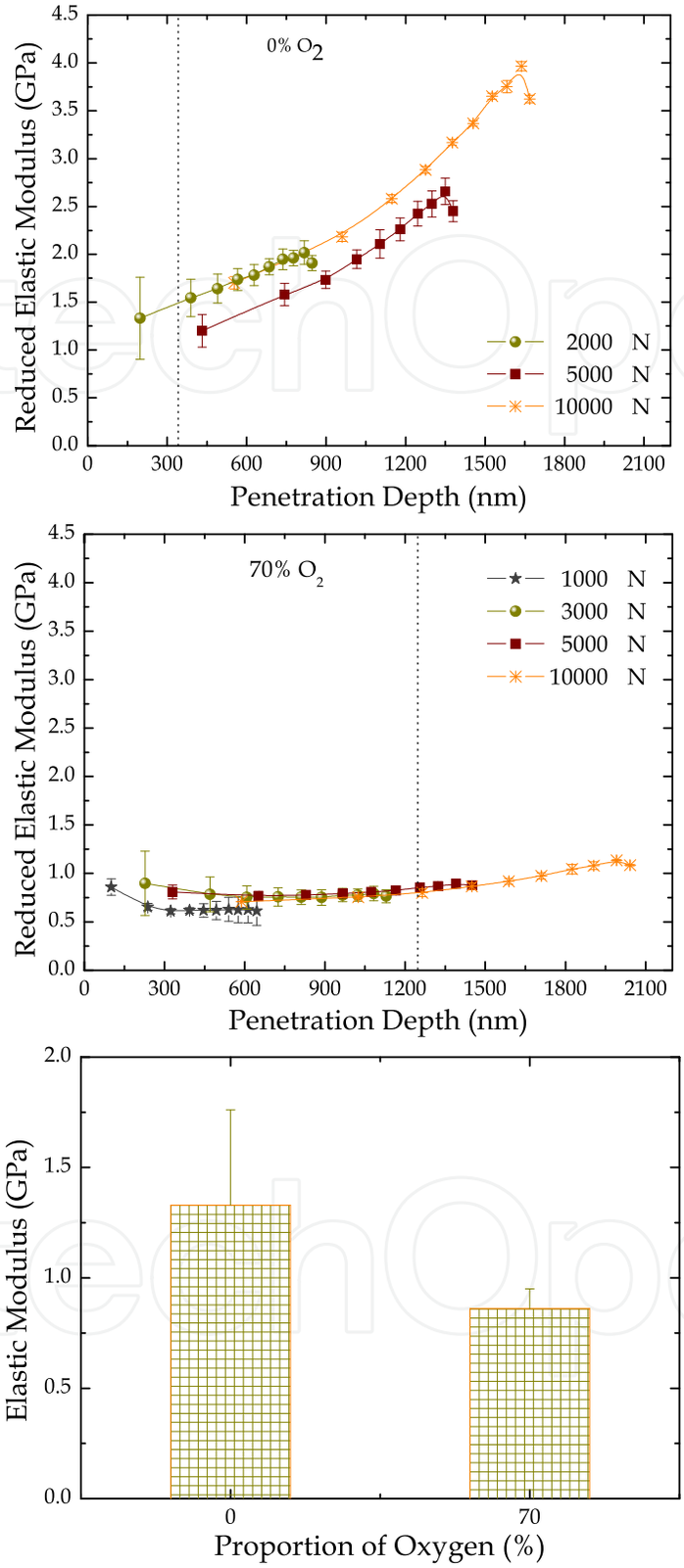

Figure 12. Elastic modulus as a function of penetration depth for films deposited using 0 and 70% of oxygen in the plasma. The vertical dotted lines in the graphs represent 15% of the total film thickness. In the lowermost graph, the elastic modulus measured at the shallowest probed depth is provided for both samples.

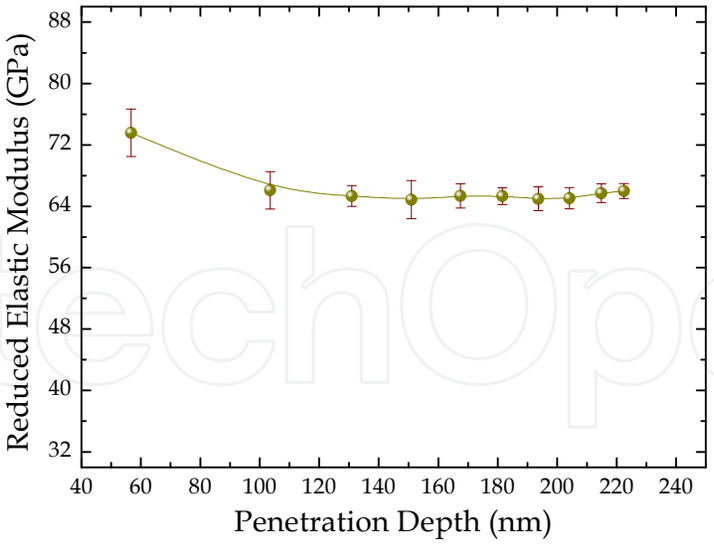

Figure 13. Reduced elastic modulus as a function of penetration depth for the glass plate used as the substrate.

It is generally accepted that wear resistance of a solid can be adjusted by tailoring its elasto-plastic properties, either by increasing H or decreasing E (Leyland & Matthews, 2000). To predict the wear resistance of the films, the elasticity index (H/E) was evaluated from data obtained at the shallowest indentation depth and is depicted in Fig. 14 as a function of the oxygen proportion. From the previous H and E results (Figs. 10 and 12) and from the H/E behavior, shown in Fig. 14, it is observed that oxygen incorporation during deposition tends to increase the wear resistance of the films. Figure 14 also depicts the resistance to plastic deformation (H^3/E^2), evaluated at the shallowest indentation depth for both samples. H^3/E^2 increases from 1.6 to 7.9 MPa as oxygen is incorporated into the plasma. Even though the elasticity index agrees well with values reported in the literature for a-Si:C:H films deposited by PECVD (Guruvenket et al., 2010), the plastic deformation resistance found here is around 50 times lower.

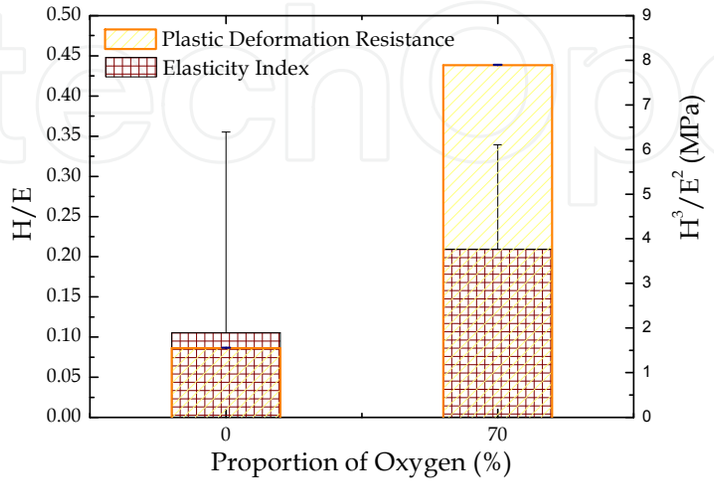

Figure 14. Elasticity index (H/E) and plastic deformation resistance (H^3/E^2) as a function of the proportion of oxygen in the depositing plasma.

According to the Johnson analysis (Tsui et al., 1995), H^3/E^2, is proportional to the load at which the material starts deforming plastically under the action of a rigid sphere of radius r. Therefore, to obtain a material highly resistant to plastic deformation H should be high and E low, consistently with the H/E parameter. This association allows the applied load to be dissipated over a larger area. On the other hand, if high plastic deformation is required, as in materials employed in nanoindentation lithography (Sirghi et al., 2009), low H^3/E^2 values are desirable. Even though the films prepared in this work resulted in low H^3/E^2 values, no residual deformation was detected after the tests, confirming that, at the loads employed here, deformation was mainly elastic due to the high H/E ratios of the films.

Therefore, from the nanoindentation results discussed here it is possible to infer that the structure gained in hardness and elasticity upon oxygen incorporation. This association improved the elasticity index and the resistance to plastic deformation, suggesting a better tribological performance of the coatings. The results indicate that even with 70% of oxygen in the mixture, carbon was effectively incorporated into the structure, resulting in a granular polymeric-like material. Oxygen has catalyzed the HMDSO deposition in the plasma environment. Still higher proportions of oxygen should be considered for the formation of a uniform oxide-like structure.

Figure 15 and 16 show SPM images of the surfaces before (left) and after (right) the wear tests. Cross-section profiles taken from specific points of the images are also presented. For the sample prepared in the pure HMDSO plasma (Fig. 15) there was no signal of wear as normal loads of up to 1000 μN were used. Slight tracks start appearing at loads greater than 1000 μN. Consistently, depressions are detected in the line profile around 19, 29 and 39 μm of the scan length, with depths increasing with the normal load. It is interesting to note, however, the preservation of the particulates over the track (3D images), suggesting a compaction of the overall tested region without material removal. For the sample deposited in the HMDSO-oxygen mixture (Fig. 16), no sign of track is detected in the images or in the cross-section profile, independently of the load used during the test. These results thus confirm the prediction of the elasticity index (Fig. 14) of a better wear resistance for the film deposited in the presence of oxygen.

Figure 17 shows the friction coefficient between the diamond nanoindenter tip and the film prepared in plasmas of HMDSO (top) and HMDSO/O_2 mixture (down). For the film deposited with no oxygen in the plasma, the friction coefficient changed from 0.1 to 0.3 along the scan length. The range of oscillation was slightly higher for the samples deposited with oxygen in the plasma, since it presented roughness values around 40% higher than the former (Fig. 6). For both samples, the major friction mechanism is attributed to the adhesion since in fully elastic deformations, this is the main interaction mode (Wang & Kato, 1998).

Figures 18 and 19 show representative scratch profiles taken from the films deposited with different proportions of oxygen in the plasma. The “Pre-scan” and “Post-scan” profiles in the graphs represent the surface condition just before and after the scratching test. Their

comparison allows inference to be made concerning the plastic deformation remaining on the scratched surface. The SPM image presented below each graph was taken immediately before (left) and after (right) the scratching experiment.

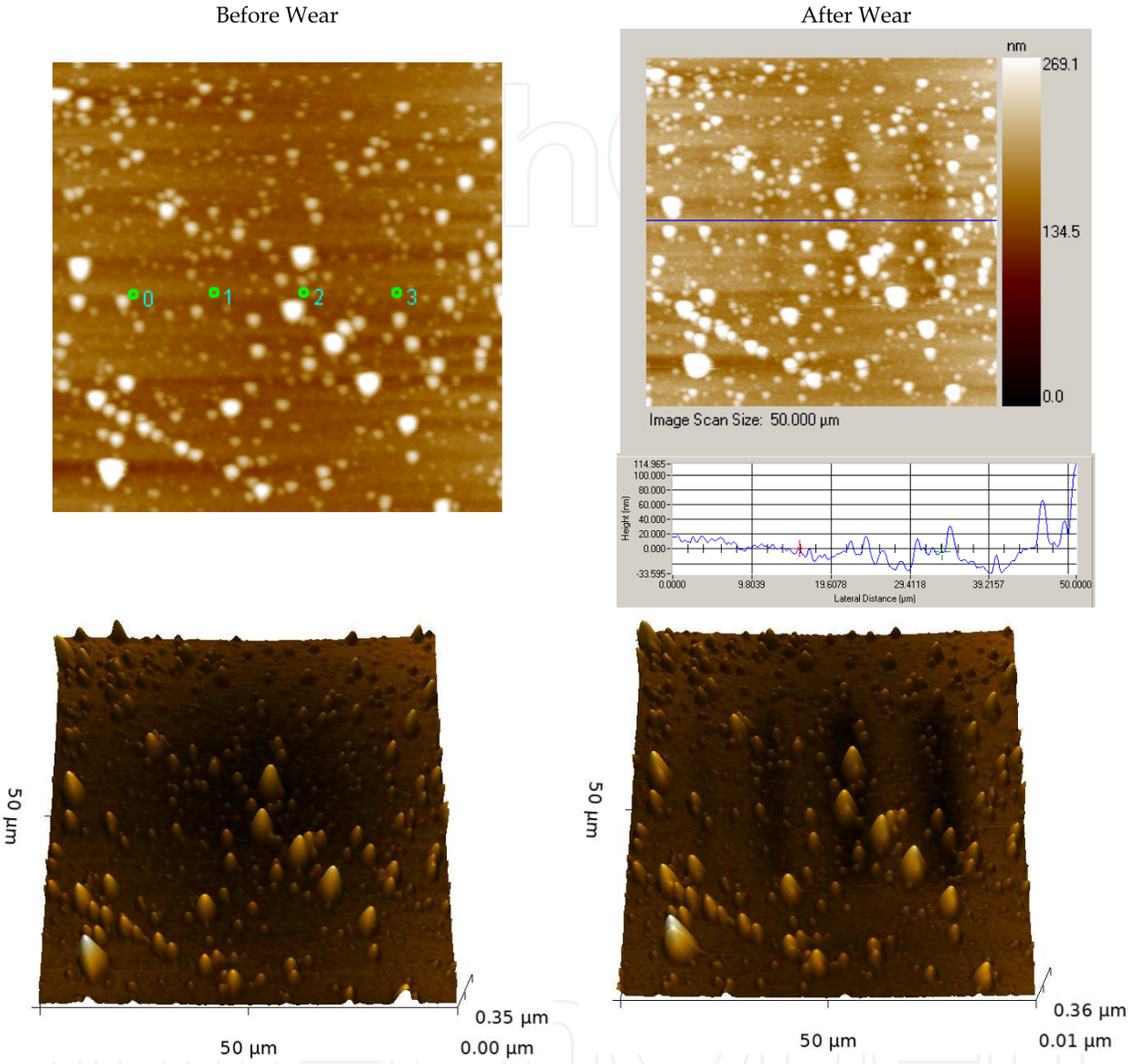

Figure 15. Bi- (top) and Tri-dimensional (bottom) scanning probe microscopy images of the film deposited in plasmas of pure HMDSO: (left) before and (right) after the wear cycle. The points in the left top image correspond to the location where the tests were conducted using 19 cycles saw-tooth function of 1000 (0), 2000 (1), 3000 (2) and 4000 µN (3) of maximum load.

All the profiles of Fig. 18 present a small slope which may be a consequence of the lack of planicity of the system. During the scratching cycle, the material undergoes deep penetration (1300 - 1100 µm) but a fast recovery is suggested by comparison of the "Scratching" and the "Post-scan" profiles, confirming the high elasticity of the structure. Interestingly, the time elapsed from the scratching test up to the end of the post-scan acquisition was only 27 s. An almost complete recovery of the deep strain produced during

the scratching test is evidenced as one compares the pre- and post- scan curves. Probably owing to the large tip diameter (~ 200 nm), no plastic deformation was observed in any region of the SPM image taken after the test

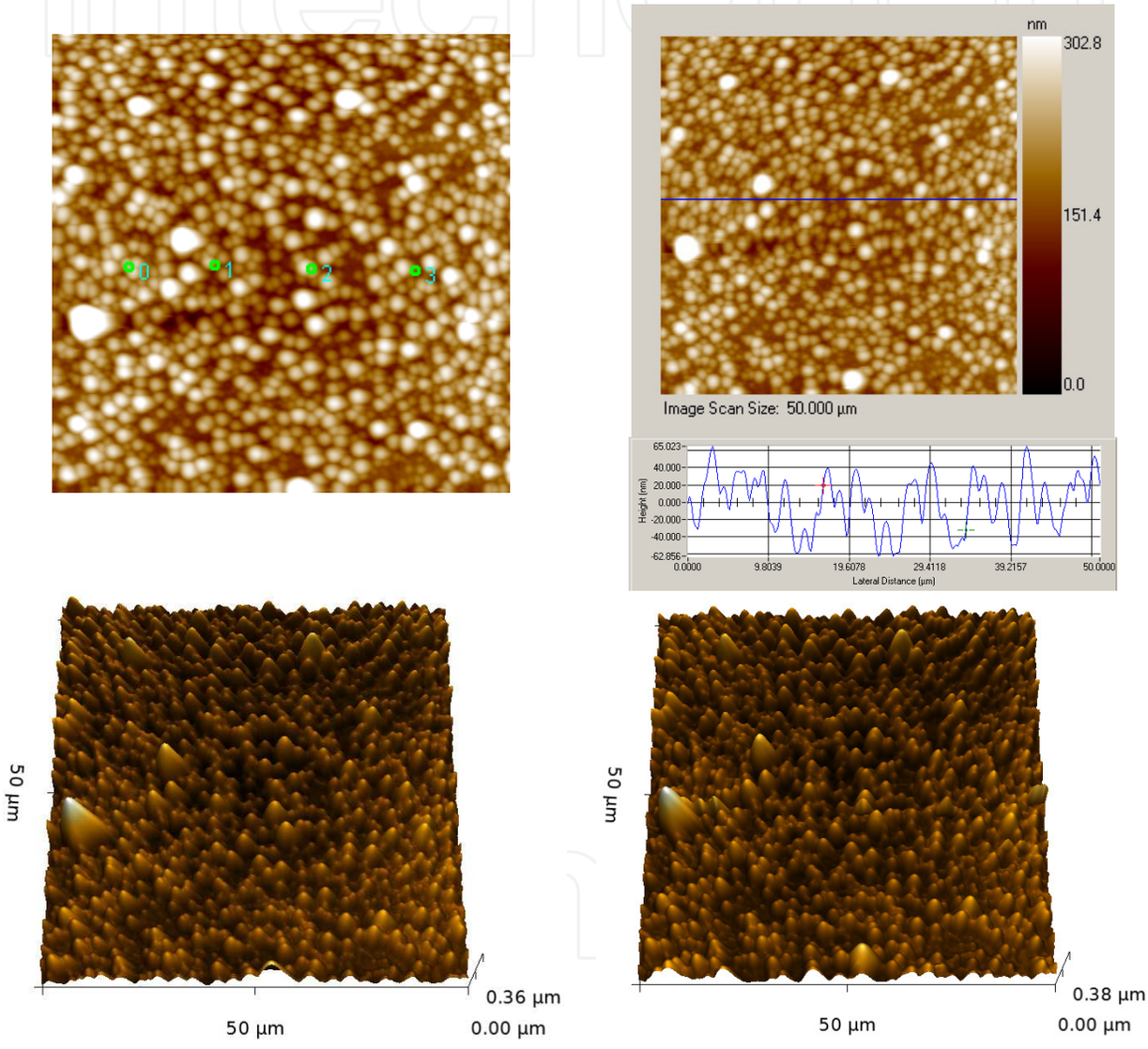

Figure 16. Bi- (top) and Tri-dimensional (bottom) scanning probe microscopy images of the film deposited in plasmas of the HMDSO/O_2 mixture: (left) before and (right) after the wear cycle. The points in the left top image correspond to the location where the tests were conducted using 19 cycles tooth saw-like function of 1000 (0), 2000 (1), 3000 (2) and 4000 µN (3) of maximum load.

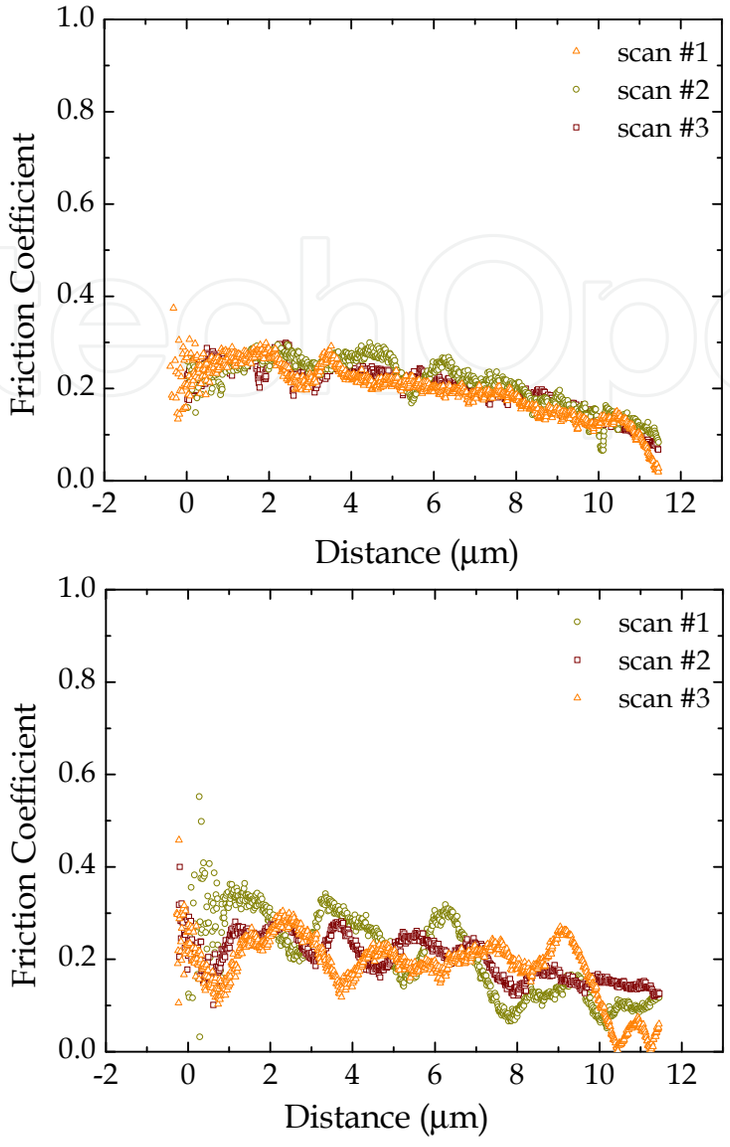

Figure 17. Friction coefficient as a function of the position for the films prepared in pure HMDSO (left) and HMDSO/O_2 (right) plasma. The scans were acquired at 300 μN of normal load and at a velocity of 1.0 μm/s.

A very similar behavior is revealed when the curves and images of Fig. 19 are considered, except that now a complete elastic recovery is seen, which is consistent with the higher elasticity index presented by this sample (Fig. 14). Although the film deposited in the presence of oxygen had a higher friction coefficient it also presented a higher scratching resistance.

Therefore, it should be pointed out that, even though a soft material was produced in any of the conditions employed here, they are wear and scratch resistant due to the high elasticity. In a general way, oxygen introduction improved the tribological properties of the films, despite the increase in the friction coefficient. The high capability of recovery of the scratched region and the low wear induced in the samples suggest the application of the films as anti-scratching coatings for a series of practical applications.

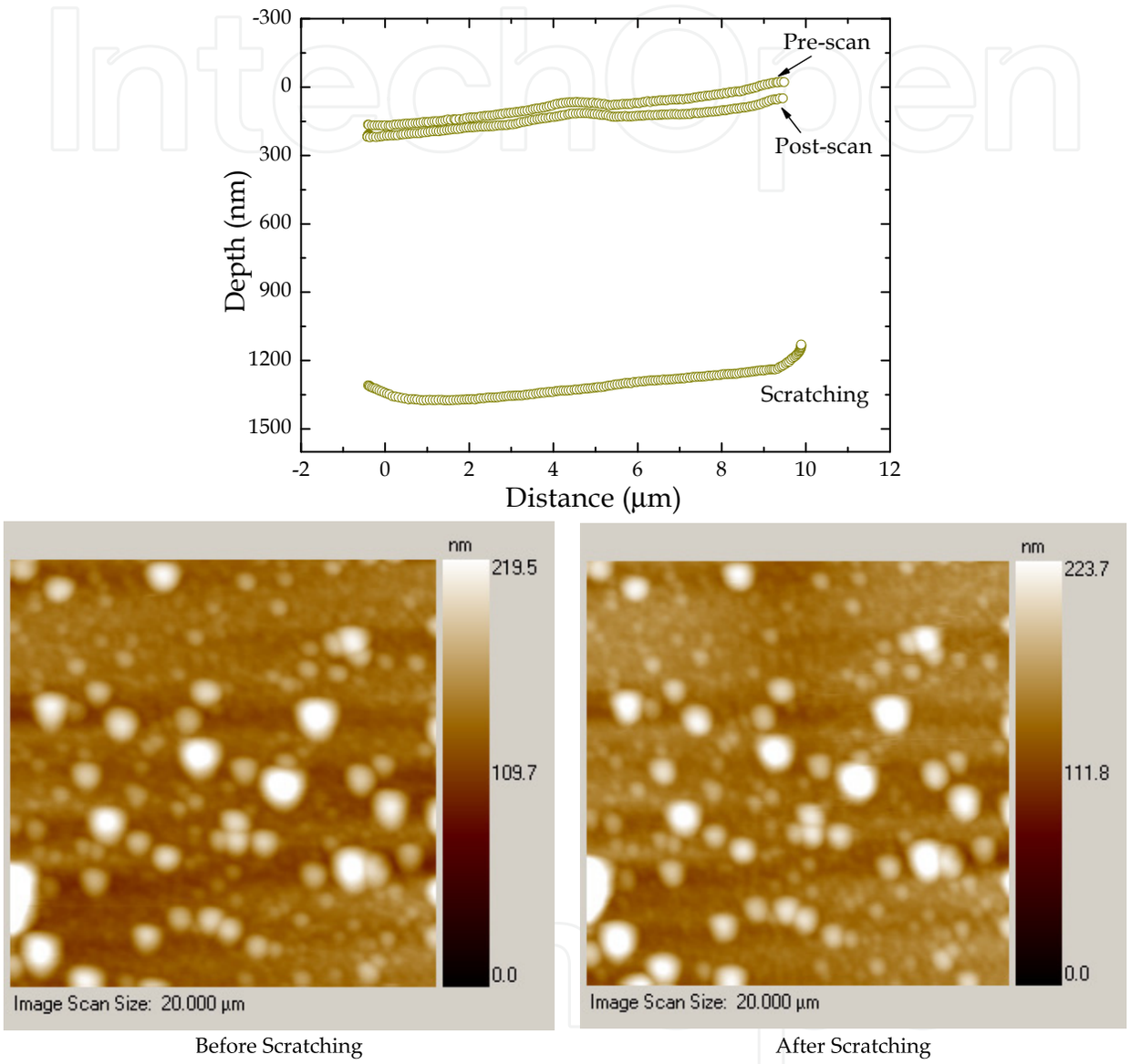

Figure 18. Profiles acquired before, during and after the scratching tests from the film deposited in a pure HMDSO plasma. The scans acquired before and after the tests were conducted with 200 µN of normal load. The lowermost pictures represent 20 X 20 mm^2 scanning probe microscopy images of the film prior (left) and after (right) the scratching tests conducted with a constant load of 5000 µN.

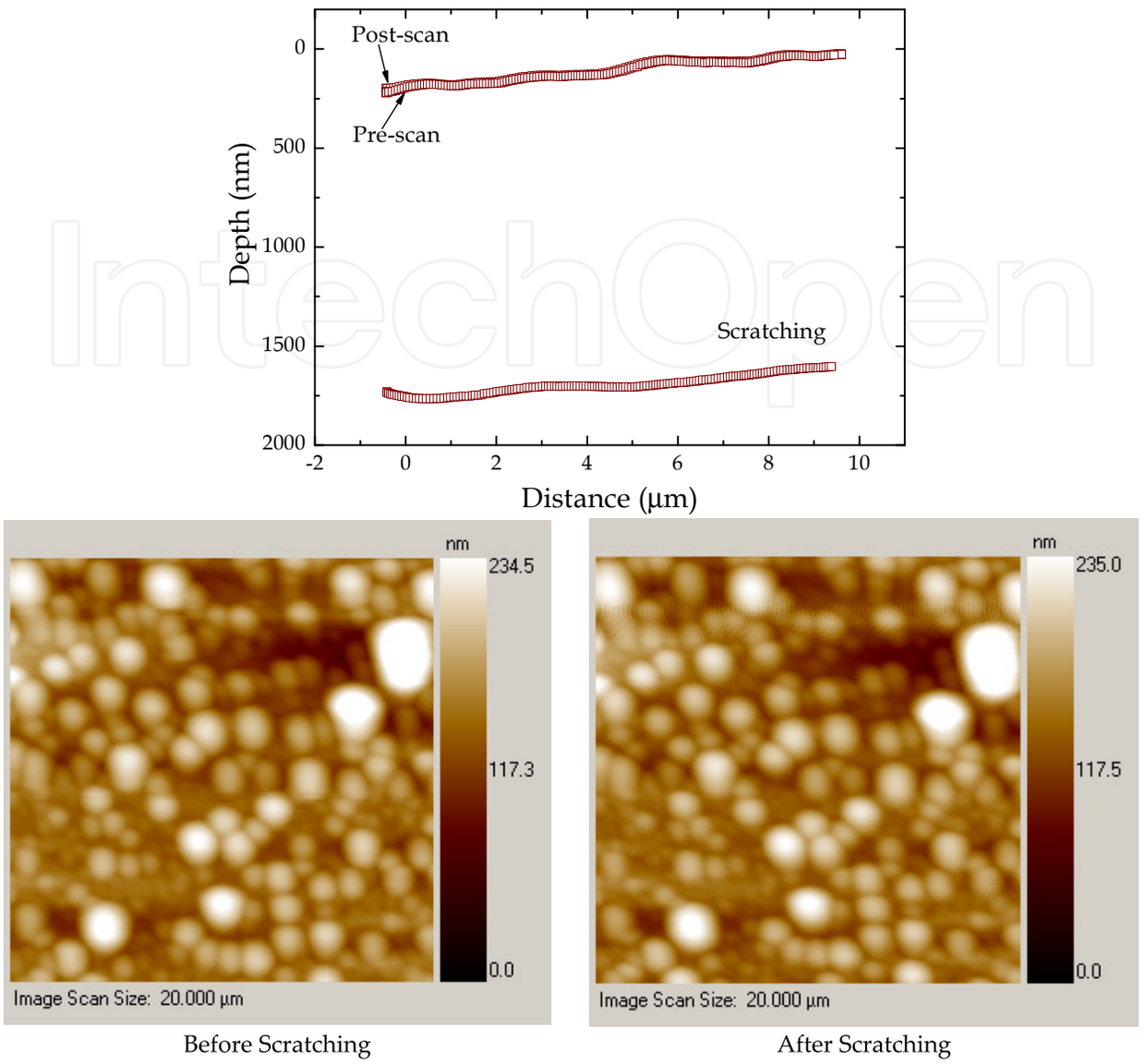

Figure 19. Profiles acquired before, during and after the scratching tests from the film prepared in the HMDSO/O_2 plasma mixture. The scans acquired before and after the test were conducted with 200 μN of normal load. The lowermost pictures represent 20 X 20 mm^2 scanning probe microscopy images of the film before and after the scratching tests conducted with a constant load of 5.000 μN.

4. Conclusion

The physical, chemical, mechanical and tribological properties of films deposited from the HMDSO precursor are dependent on the oxygen proportion in the plasma phase. The proportion of oxide inclusions increased upon oxygen incorporation, enhancing hardness and decreasing elastic modulus. Friction slightly increased due to better adhesion of the surfaces promoted by chemical and topographical alterations. Independently of the deposition condition, films are scratch and wear resistant due to the high elasticity of the structure. The coating with best tribological performance was produced as oxygen was incorporated during the deposition process. Associating the results obtained for the

chemical structure with the mechanical and tribological properties it was possible to infer the polymeric nature of the coatings. Still higher oxygen proportions should be necessary to effectively scavenge carbon from the structure during depositions. In the proportion used here, however, oxygen played a crucial role in the plasma kinetics since it increased the deposition rate and the coalescence of particulates in the plasma, affecting the overall structure of the film. Furthermore, the indentation, scratching and images capabilities of the nanoindenter employed as well as of the nanoindentation theory were shown to provide important results or predictions of the material properties on the nanometric scale. The determination of the mechanical and tribological properties of the films revealed their potential, despite their initially being investigated specifically owing to their excellent corrosion barrier properties, as anti-scratch transparent coatings for optical devices.

Author details

Bruno B. Lopes, Rita C.C. Rangel, César A. Antonio,
Steven F. Durrant, Nilson C. Cruz, Elidiane C. Rangel
São Paulo State University, Brazil

Acknowledgement

The authors would like to thank Brazilian agencies FAPESP and CNPq for financial support.

5. References

Bewilogua, K.; Bialuch, I.; Ruske, H. & Weigel, K. (2011). Preparation of a-C:H/a-C:H:Si:O and a-C:H/a-C:H:Si multilayer coatings by PACVD. *Surface & Coatings Technology.* 2011, Vol. 206, 4, pp. 623–629

Borvon, G.; Goullet, A.; Mellhaoui, X.; Charrouf, N. & Granier, A. (2002). Electrical properties of low-dielectric-constant films prepared by PECVD in O_2/CH_4/HMDSO. *Materials Science in Semiconductor Processing*. Apr-Jun 2002, Vol. 5, 2-3, pp. 279-284

Boscher, N.D.; Choquet, P.; Duday, D. & Verdier, S. (2010). Chemical compositions of organosilicon thin films deposited on aluminium foil by atmospheric pressure dielectric barrier discharge and their electrochemical behaviour. *Surface & Coatings Technology.* Dec 2010, Vol. 205, 7, pp. 2438–2448

Choudhury, A.J.; Chutia, J.; Kakati, H.; Barve, S.A.; Pal, A.R.; Sarma, N.S.; Chowdhury, D. & Patil, D.S. (2010). Studies of radiofrequency plasma deposition of hexamethyldisiloxane films and their thermal stability and corrosion resistance behavior. *Vacuum.* Jun 2010, Vol. 84, 11, pp. 1327-1333

Choudhury, A.J.; Barve, S.A.; Chutia, J.; Pal, A.R.; Kishore, R.; Jagannath; Pande, M. & Patil, D.S. (2011). RF-PACVD of water repellent and protective HMDSO coatings on bell metal surfaces: Correlation between discharge parameters and film properties. *Appl. Surf. Sci.* Aug 2011, Vol. 257, 1, pp. 8469-8477

Czeremuszkin, G.; Latreche, M.; Wertheimer, M.R. & Sobrinho da Silva, A.S. (2001). Ultrathin Silicon-Compound Barrier Coatings for Polymeric Packaging Materials: An Industrial Perspective. *Plasmas Polym.* Jun 2001, Vol. 6, 1-2, pp. 107-120

Fracassi, F.; d'Agostino, R.; Palumbo, F.; Angelini, E.; Grassini, S. & Rosalbino, F. (2003). Application of plasma deposited organosilicon thin films for the corrosion protection of metals. *Surface and Coatings Technology*, Sep-Oct 2003, Vol. 174–175, pp. 107-111

Gengenbach, T.R. & Griesser, H.J. (1999). Post-deposition ageing reactions differ markedly between plasma polymers deposited from siloxane and silazane monomers. *Polymer*. Aug 1999, Vol. 40, 18, pp. 5079-5094

Görbig, O.; Nehlsen, S. & Mtiller, J. (1998). Hydrophobic properties of plasma polymerized thin film gas selective membranes. *Journal of Membrane Science*. Jan 1998, Vol. 138, 1, pp. 115-121

Guruvenket, S.; Azzi, M.; Li, D.; Szpunar, J.A.; Martinu, L. & Klemberg-Sapieha, J.E. (2010). Structural, mechanical, tribological, and corrosion properties of a-SiC:H coatings prepared by PECVD. *Surface & Coatings Technology*. Aug 2010, Vol. 204, 21-22, pp. 3358–3365

Jin, S.B.; Lee, J.S.; Choi, Y.S.; Choi, I.S. & Han, J.G. (2011). High-rate deposition and mechanical properties of SiO(x) film at low temperature by plasma enhanced chemical vapor deposition with the dual frequencies ultra high frequency and high frequency. *Thin Solid Films.* Jul 2011, Vol. 519, 19, pp. 6334–6338

Leyland, A. & Matthews, A. (2000). On the significance of the H/E ratio in wear control: a nanocomposite coating approach to optimised tribological behaviour. *Wear*. Nov 2000, Vol. 246, 1-2, pp. 1–11

Morent, R.; Geyter, N.D.; Vlierberghe, S.V.; Dubruel, P.; Leys, C. & Schacht, E. (2009). Organic-inorganic behaviour of HMDSO films plasma-polymerized at atmospheric pressure. *Surface and Coatings Technology*. Feb 2009, Vol. 203, 10-11, pp. 1366-1372

Navabpour, P.; Teer, D.; Su, X.; Liu, C.; Wang, S.; Zhao, Q.; Donik, C.; Kocijan, A. & Jenko, M. (2010). Optimisation of the properties of siloxane coatings as anti-biofouling coatings: Comparison of PACVD and hybrid PACVD-PVD coatings. *Surface and Coatings Technology*. Jul 2010, Vol. 204, 20, pp. 3188-3195

Oliver, W.C.; Pharr, G.M. (1992). An improved technique for determining hardness and elastic modulus using load and displacement sensing indentation experiments. *Journal of Material Research*. Jan 1992, Vol. 7, 6, pp. 1564-1583.

Ong, S.E.; Zhang, S.; Du, H.; Too, H.C. & Aung, K.N. (2007). Influence of silicon concentration on the haemocompatibility of amorphous carbon. *Biomaterials.* Oct 2007, Vol. 28, 28, pp. 4033-4038

Ong, S.E.; Zhang, S.; Du, H.; Wang, Y. & Ma, L.L. (2008). In-vitro cellular behavior on amorphous carbon containing silicon. *Thin Solid Films.* Jun 2008, Vol. 516, 16, pp. 5152-5156

Pfuch, A.; Heft, A.; Weidl, R. & Lang, K. (2006). Characterization of SiO2 thin films prepared by plasma-activated chemical vapour deposition. *Surface & Coating Technology.* Sep 2006, Vol. 201, 1-2, pp.189-196

Pihan, S.A.; Tsukruk, T. & Förch, R. (2009). Plasma polymerized hexamethyl disiloxane in adhesion applications. *Surface and Coatings Technology*. Mar 2009, Vol. 203, 13, pp. 1856-1862

Quédé, A.; Jama, C.; Supiot, P.; Le Bras, M.; Delobel, R.; Dessaux, O. & Goudmand, P. (2002). Elaboration of fire retardant coatings on polyamide-6 using a cold plasma polymerization process. *Surface and Coatings Technology*. Mar 2002, Vol. 151–152, pp. 424-428

Rangel, R.C.C.; Pompeu, T.C.; Barros Jr., J.L.S.; Antonio, C.A.; Santos, N.M.; Pelici, B.O.; Freire, C.M.A.; Cruz, N.C. & Rangel, E.C. (2012). Improvement of the Corrosion Resistance of Carbon Steel by Plasma Deposited Thin Films, In: *Recent Researches in Corrosion Evaluation and Protection*, Reza Shoja Razavi, pp. 91-116, Intech Open Access Publisher, Retrieved from http://www.intechopen.com/articles/show/title/improvement-of-the-corrosion-resistance-of-carbon-steel-by-plasma-deposited-thin-films

Ricci, M.; Dorier, J.; Hollestein, C. & Fayet, P. (2011). Influence of Argon and Nitrogen Admixture in HMDSO/O2 Plasmas onto Powder Formation. *Plasma Process. Polym.* Feb 2011, Vol. 8, 2, pp. 108-117

Rouessac, V.; Ungureanu, A.; Bangarda, S.; Deratani, A.; Lo, C.; Wei, T.; Lee, K. & Lai, J. (2011). Fluorine-Free Superhydrophobic Microstructured Films Grown by PECVD. *Chemical Vapor Deposition*. Sep 2011, Vol. 17, 7-9, pp. 198–203

Schilde, C.; Westphal, B.; Kwade, A. (2012). Effect of the primary particle morphology on the micromechanical properties of nanostructured alumina agglomerates. *J. Nanopart. Res*. Feb 2012, Vol 14, 3, pp.1-11.

Schwarz, J.; Schmidt, M. & Ohl, A. (1998). Synthesis of plasma-polymerized hexamethyldisiloxane (HMDSO) films by microwave discharge. *Surface and Coatings Technology*. Jan 1998, Vol. 98, 1-3, pp. 859-864

Sirghi, L.; Ruiz, A. ; Colpo, P. & Rossi, F. (2009). Atomic force microscopy indentation of fluorocarbon thin films fabricated by plasma enhanced chemical deposition at low radio frequency power. *Thin Solid Films.* Apr 2009, Vol. 517, 11, pp. 3310–3314

Tsui, T.Y. ; Pharr, G.M.; Oliver, W.C.; Bhatia, C.S.; White, R.L.; Anders, S.; Anders, A. & Brown, I.G. (1995). Nanoindentation and nanoscratching of hard carbon coatings for magnetic disks. *Material Research Society Symposium Procedings*. 1995, Vol. 383, pp. 447-452

Ul, C.V.; Laporte, C.B.; Benissad, N.; Chausse, A.; Leprince, P. & Messina, R. (2000). Plasma-polymerized coatings using HMDSO precursor for iron protection. *Progress in Organic Coatings*. Feb 2000, Vol. 38, 1, pp. 9-15

Ul, C.V.; Roux, F.; Laporte, C.B.; Pastol, J.L. & Chausse, A. (2002). Hexamethyldisiloxane (HMDSO)-plasma polymerised coatings as primer for iron corrosion protection: influence of RF bias. *J. Mater. Chem.* Jun 2002, Vol. 12, 8, pp. 2318-2324

Wang, D. F. & Kato, K. (1998). Friction studies of ion beam assisted carbon nitride coating sliding against diamond pin in water vapor. *Wear*. May 1998, Vol. 217, 2, pp. 307-311

Zajíčková, L.; Buršíková, V.; Peřina, V.; Macková, A.; Subedi, D.; Janča, J. & Smirnov, S. (2001). Plasma modification of polycarbonates. *Surface and Coatings Technology*. Jul 2001, Vol. 142–144, pp. 449-454